Optics Communications 342 (2015) 20–25

Contents lists available at ScienceDirect

Optics Communications

journal homepage: www.elsevier.com/locate/optcom

Ultrathin dual-mode filtering characteristics of terahertz metamaterials with electrically unconnected and connected U-shaped resonators array

Zhaoxiang Cheng, Lin Chen *, Xiaofei Zang, Bin Cai, Yan Peng, Yiming Zhu *

Shanghai Key Lab of Modern Optical System, Engineering Research Center of Optical Instrument and System, Ministry of Education, University of Shanghai for Science and Technology, No. 516 JunGong Road, Shanghai 200093, China

ARTICLE INFO

Article history:
Received 15 October 2014
Received in revised form
8 December 2014
Accepted 14 December 2014
Available online 17 December 2014

Keywords:
Metamaterials
Terahertz
Polarization
Filter
Modulator

ABSTRACT

We experimentally and numerically demonstrate dual-mode resonances of electrically unconnected and connected U-shaped resonators array on flexible polyimide substrate in terahertz (THz) region. The unit cell consisting of two back-to-back U-shaped resonators (TUR) shows strong induction-capacitance resonance for TM mode and dipole resonance for TE mode. Then we clarify the transmission spectra characteristics of fourfold U-shaped resonators (FURs), which are composed of two twisted TUR at 90°. Distinct characteristic transmission responses are observed in varied coupled distances, specially, an "L-shaped" resonance is observed at connected FUR which does not exist in unconnected FUR. The polarization tunable property of TUR and polarization-independent characteristics of FUR are adequately clarified. Some applications such as polarization-tunable modulator (peak-to-peak value is about 0.4 for 90° polarization rotation) and polarization-independent dual-channel filter (full width with half maximum (FWHMs) nears to 85 GHz) is proposed and verified experimentally, which may benefit to broaden novel ultrathin flexible THz devices.

1. Introduction

THz technology has attracted a lot of research interest during the past decades, which attributes to the rapid progress in THz emitters, detectors, and functional components [1–7]. Among these progresses, THz metamaterials have gained widely attentions over the past decade due to their fantastic characteristics and potential applications such as negative refractive index [8,9], absorbers [10,11], superlens [12], and sensing [13,14]. The split ring resonator (SRR) is one of the most popular elements to construct metamaterials due to its simplicity and easy understanding by using induction-capacitance (LC) theory. Specially, a U-shaped resonator (UR) which is simplified by SRR is a much more fundamental metamaterials element. Many phenomena based on complex structures can be easily understood in metamaterials with simple UR arrays. In addition, a large number of designs can be achieved in coupled UR arrays by varying the mutual resonator-resonator coupling strength, which modifies the resonant frequencies and field intensities of coupled UR arrays [15–17]. To directly understanding the origin of such UR arrays interaction, some work focus on the effects of coupling for two fundamental geometrical array layout schemes, in which two URs are placed back to back or face to face [18,19]. The asymmetric configuration and the coupling strength are sufficiently studied to analysis the resonance hybridization. In our previous work, a switchable polarization sensitive THz metamaterials filter was proposed, which consisted of four square electric LC structures and two connecting bent-lines on a flexible substrate [20]. In this paper, we theoretically proposed and experimentally verified a novel metamaterials for similar modulation purpose in Ref. [20]. Different from the structure in Ref. [20], our designed structure comprises two U-shaped resonators (TUR) which are placed back-to-back. This structure reflects different responses and resonances for TE and TM polarized wave. By using this structure, a polarization-tunable switchable modulator could be realized, which experimental peak-to-peak value of normalized transmission is about 0.4 for 90° polarization rotation. Furthermore, by borrowing the polarization insensitive arrangement proposed in Ref. [21] which detects the electromagnetically induced transparency (EIT) with a windmill type metamaterial consisting of two dumbbell dielectric resonator, we also demonstrated polarization insensitive property with a "fourfold U-shaped resonators" (FUR) unit cell composed of two orthogonal back placed TUR. The transmission property of coupled UR arrays (coupling between adjacent URs in FUR) are important

* Corresponding authors. Fax: +86 21 33773176.
E-mail addresses: linchen@usst.edu.cn (L. Chen), ymzhu@usst.edu.cn (Y. Zhu).

http://dx.doi.org/10.1016/j.optcom.2014.12.042
0030-4018/

and need to be researched; even the transmission effect of single UR structures have been theoretically analyzed [22]. The transmission responses and coupled mechanisms of different distances varied from unconnected to point-contacted and finally fully connected FUR are completely researched. Different resonance properties are observed in the unconnected FUR (UFUR), point-contacted FUR (PFUR) and connected FUR (CFUR). Specially, an "L-shaped" resonance is observed in PFUR and CFUR which does not exist in UFUR. As their polarization insensitive properties, the UFUR and CFUR both can be designed as a polarization-independent dual-channel filter. The measured full width with half maximum (FWHM) are about 90 GHz and 80 GHz at the two dips for UFUR, while the FWHM of CFUR are 130 GHz and 75 GHz. Due to their tunable and flexible properties, our metamaterials could be widely used in THz field.

2. Fabrication and results

The designed metamaterials are illustrated in Fig. 1. The unit cell of FUR is comprised of two identical TUR twisted by 90°. Geometric parameters of FUR are depicted in Fig. 1(a), with arm length $a=100$ μm, gap length $b=60$ μm, groove depth $h=80$ μm, line width $w=20$ μm, the distance between two adjacent URs $s=10$ μm, and the period of unit cell $p=380$ μm. The metamaterials were fabricated with 200 nm thick aluminum film on a 25 μm thick flexible polyimide substrate by conventional photolithography [21]. In Fig. 1(b), I, II, and III are the optical microscope images of the TUR, UFUR and CFUR samples, respectively, IV is the photograph of the flexible thin polyimide substrate. The planar samples were measured by use of fast and slow scan-based THz time domain spectroscopy (THz-TDS) [23–25]. The absolute amplitude transmittance is defined as $|t(\omega)|=|E_S(\omega)/E_R(\omega)|^2$, where $E_S(\omega)$ and $E_R(\omega)$ are Fourier transformed amplitudes of the THz pulse transmitted through the samples and reference (the blank polyimide substrate), respectively.

At the first step, we investigate the transmission responses of back coupled TUR excited by normal incident electromagnetic wave with 0° polarization angle (TM wave) and 90° polarization angle (TE wave). The experimental and simulated results are presented in Fig. 2(a) and (b), respectively. The measured data are supported by full-wave numerical simulations using CST Microwave Studio. The polyimide substrate with relative permittivity $\varepsilon_{pi}=3.5$ is modeled as a lossy dielectric medium with a loss tangent of 0.05 and aluminum is simulated with a conductivity of $\sigma_{Al}=3.56\times 107$ S/m

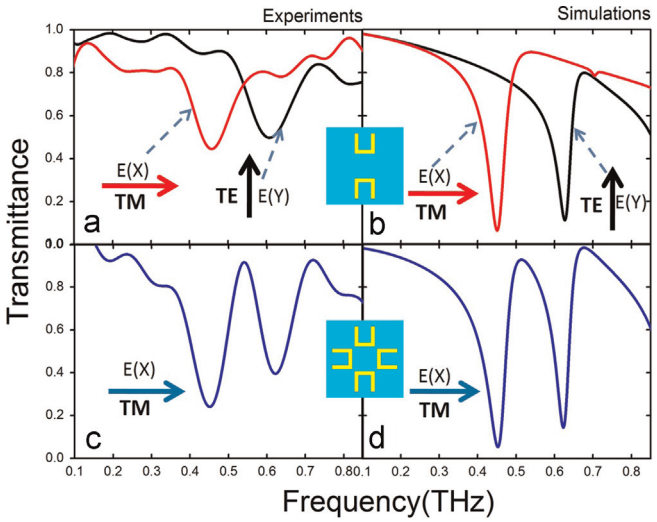

Fig. 2. (a) Experimental and (b) simulated transmission spectra of TUR excited by TM polarized wave (red line) and TE polarized wave (black line). (c) Experimental and (d) simulated transmission spectra of UFUR under TM polarized wave excitation. (For interpretation of the references to color in this figure legend, the reader is referred to the web version of this article.)

(behave almost like perfect conductor compared to visible region [26]). When the back placed TUR is excited by TM polarized wave, (see red curves in Fig. 2(a) and (b)), a transmission dip occurs at 0.451 THz. However, when the incident electric field turns to TE mode, another resonance dip emerges at 0.627 THz, and the original resonance dip disappears completely (see as the black curve in Fig. 2(a) and (b)). Here, the back placed TUR array can also be regarded as the face coupled TUR array, but the response for the face placed TUR is the same as that for the back coupled TUR array. It is because that in our design the coupling effect between two URs (either face coupled or back coupled) is extremely weak due to far distance and symmetric structure. To further explore the characteristic transmission responses of two twisted TURs, the spectral transmittance of UFUR evoked by TM polarized wave are shown in Fig.2(c) and (d). It notes that there is no difference between TM mode and TE mode for UFUR as its symmetric nature. It is observed that two dips produced at 0.452 THz and 0.623 THz, which come from the combined resonance effects of perpendicular and parallel oriented TURs. The experimental and simulated spectra fit very well, except some difference of the amplitude intensity which caused by the absorption loss of substrate material.

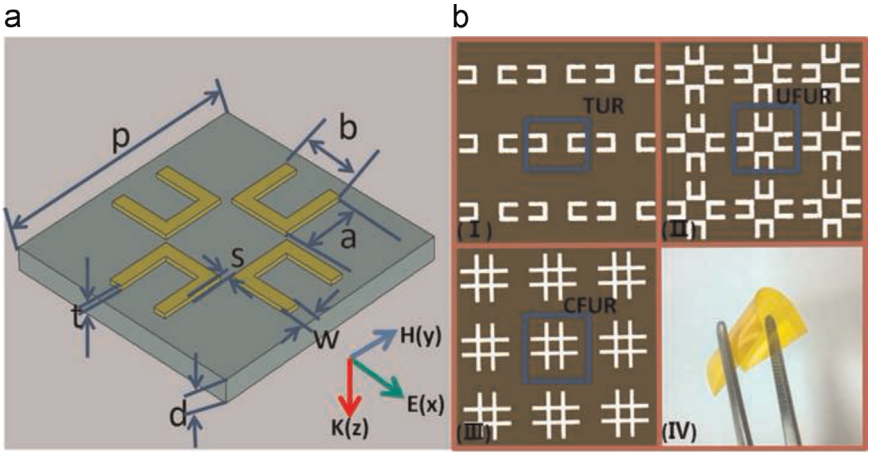

Fig. 1. (a) The unit cell of FUR, with arm length $a=100$ μm, gap length $b=60$ μm, groove depth $h=80$ μm, line width $w=20$ μm, the distance between URs $s=10$ μm, and the period of unit cell $p=380$ μm. (b) I, II, and III, are the optical microscope images of the UTUR, PFUR and CFUR samples, respectively, IV is the photograph of the flexible thin polyimide substrate.

3. Analysis and discussion

To understand the origin of the spectral characteristics, electric field and surface currents distributions of TUR and UFUR are given in Fig. 3(a) and (b), respectively. In Fig. 3(a), I and II show the electric field and surface currents distributions, respectively, at low-frequency resonance dip (0.451 THz) of TUR with a TM polarized incident wave. It is clear that the resonance dip arises from the induction-capacitance (LC) resonance [19]. When the incident electric field converts to TE polarized mode, the resonance frequency moves to 0.627 THz and acts as a dipole resonance, see III and IV in Fig. 3(a). Indeed, the TUR can be regarded as a bar resonator for TM mode and LC resonator for TE mode. In UFUR, the low-frequency resonance dip located at 0.452 THz is dominated by the LC resonance in the perpendicular arranged TUR (shown in Fig. 3(b), I and II) and the high-frequency resonance dip located at 0.623 THz primarily arises from the dipole resonance in parallel oriented TUR (shown in Fig. 3(b), V and VI). In the transparency peak 0.530 THz, the LC resonance and dipole resonance exist at the same time with comparative electric field intensity (weaker than the resonances at two dips, presented by the light red arrows in Fig. 3(b)), meanwhile the direction of surface currents are opposite at the two twisted TURs (shown in Fig. 3(b), III and IV). At the transparency window 0.53 THz, the weak destructive interference between adjacent URs can be found in Fig. 3(b) III.

To further clarify the resonance properties of FUR, we also study the transmission spectra of different coupled distances s, varied from $s=10$ μm (UFUR), $s=0$ μm (PFUR) and $s=-20$ μm (CFUR), as shown in Fig. 4(a). Fig. 4(b) is the image of FURs with different distances s. When coupled distance s decreased from 10 μm to 0 μm, the resonance dips of UFUR at 0.452 THz and 0.623 THz disappeared, meanwhile another two new resonance dips emerge at 0.36 THz (a broad resonance dip) and 0.50 THz (a sharp resonance dip). Further, when the four URs are fully connected ($s=-20$ μm), two strong resonances exist at 0.38 THz and 0.56 THz. Compared with UFUR, the CFUR owns an intense and broad resonance at the low-frequency dip. Meanwhile, the CFUR exhibits a stronger resonance at the high-frequency dip than PFUR.

To understand the underling physics of the transmission spectra with PFUR and CFUR, the electric field and surface currents distributions at corresponding resonance dips are given in Fig. 5. In PFUR, the low-frequency resonance dip is mainly driven by the LC resonance on perpendicular TUR, see (I) and (II) in Fig. 5(a). The high-frequency resonance dip primary arises from the "L-shaped" resonance of adjacent arms, meanwhile an anti-phase surface currents appear at the perpendicular arrayed TUR, as shown in Fig. 5(a) (III) and (IV). From the surface currents distributions, it indicates that two twisted TURs are electrically connected even just four point contact among adjacent URs. Importantly, the "L-shaped" resonance could not be discovered in UFUR. To further research the mechanism of electrically connected FUR, the resonance property of CFUR are described below. The low-frequency resonance dip is mostly induced by the LC resonance on perpendicular TUR and another dip is created by the "L-shaped" resonance, as in Fig. 5(b). It is notable that the "L-shaped" resonance in CFUR is stronger than PFUR, meanwhile the anti-phase surface currents at the high-frequency dip disappears, which is consistent with the observed transmission spectrum as illustrated in Fig. 4(a). Compared with UFUR, the CFUR have stronger LC resonance at the low-frequency dip, meanwhile an "L-shaped" resonance is observed at the high-frequency dip which does not exist in UFUR. Therefore, distinct characteristic transmission responses are observed at varied coupled distance, which is owning to different modes take place at unconnected and connected FUR.

4. Two applications

4.1. Polarization-tunable switchable modulator based on TUR array

Here, we analyse the transmission responses of back coupled TUR excited by different polarization electric fields as shown in Fig. 6. Fig. 6(a) and (b) are the simulated and experimental transmission spectra via different polarization angles θ, respectively. When the TUR is excited by TM polarized wave, namely $\theta=0°$, only one dip exists in 0.452 THz which arises from the LC resonance. With the increase of the polarization angle θ, the resonance intensity at this dip becomes weak and finally disappears when θ approaches to 45°, meanwhile a new dip emerges at 0.627 THz and becomes strong step by step. The high-frequency dip is a dipole resonance which is studied above. Therefore, under the TM polarized wave ($\theta=0°$), the low-frequency resonance dip located at 0.451 THz puts out the characteristics of stop band, which can be regarded as switch-off state, meanwhile the high-frequency resonance dip at 0.627 THz fully permits the electromagnetic wave transmission, which acts as a switch-on state. When the incident electromagnetic wave changes to TE mode ($\theta=90°$), the result shows opposite effect. Consequently, the conversion of on–off state between the two modes can be achieved with different polarization angles. In the experiment, the different polarization angles could be easily realized by rotating the samples. The experimental peak-to-peak value is about 0.4. As its polarization-dependent property, the TUR could be used as a polarization-tunable switchable modulator.

4.2. Polarization-independent dual-channel filers based on UFUR and CFUR

We have already discussed the transmission characteristics of TUR array, which presents the feature of switchable modulation

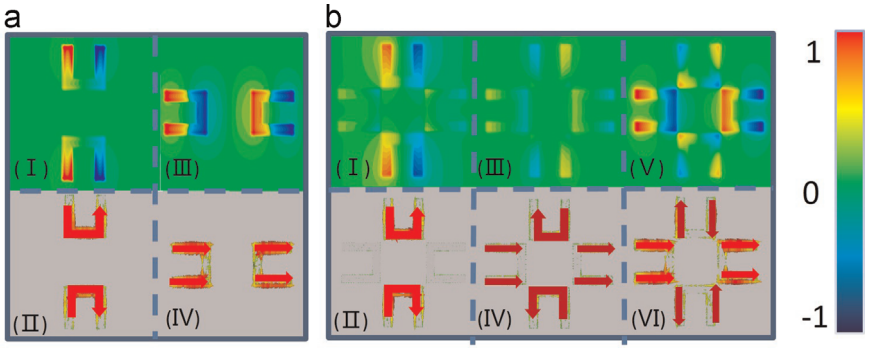

Fig. 3. (a) The electric field and surface currents distributions of (a) TUR (I) and (II) at 0.451 THz excited by a TM polarized wave, (III) and (IV) at 0.627 THz under a TE polarized wave, and (b) UFUR (I) and (II) at 0.452 THz (the low-frequency resonance dip), (III) and (IV) at 0.530 THz (the transparency peak), (V) and (VI) at 0.623 THz (the high-frequency resonance dip). (For interpretation of the references to color in this figure legend, the reader is referred to the web version of this article.)

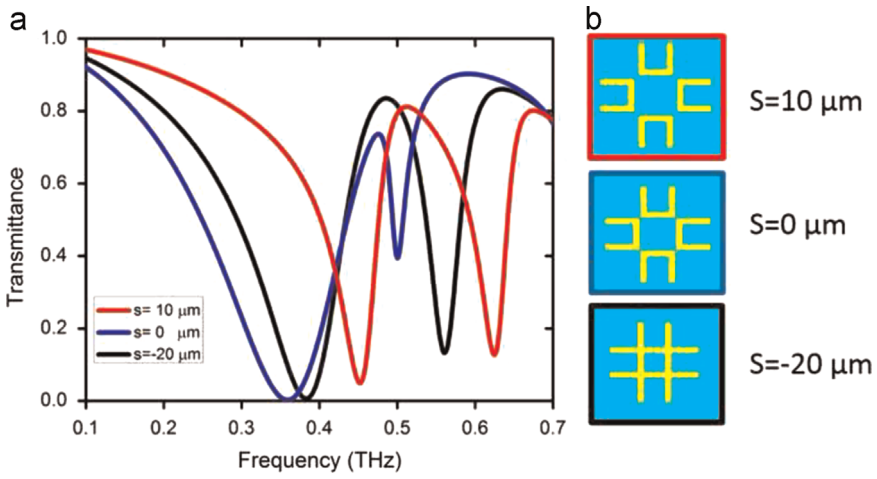

Fig. 4. (a) Transmission spectra of different coupled distances s varied from $s=10$ μm (UFUR, red line) to $s=0$ μm (PFUR, blue line) and finally $s=-20$ μm (CFUR, black line). (For interpretation of the references to color in this figure legend, the reader is referred to the web version of this article.)

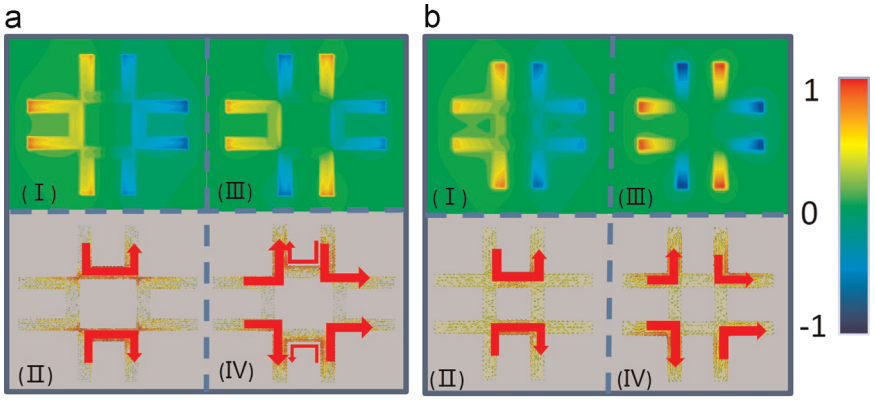

Fig. 5. The electric field and surface currents distributions of (a) UFUR I and II at low-frequency resonance dip 0.36 THz, III and IV at high-frequency resonance dip 0.50 THz, and (b) CFUR I and II at low-frequency resonance dip 0.38 THz, III and IV at high-frequency resonance dip 0.56 THz.

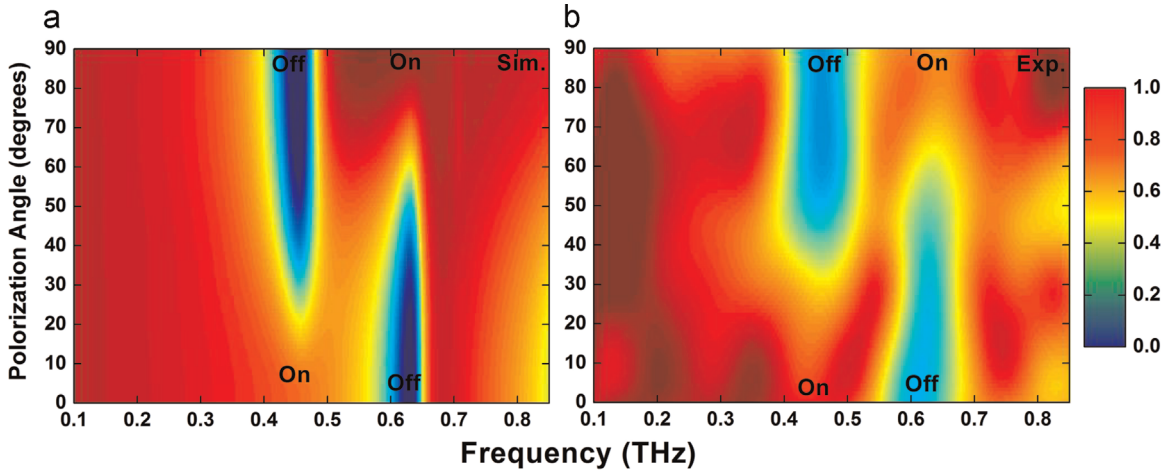

Fig. 6. (a) Simulated and (b) experimental transmission spectra of TUR with different polarization angles θ.

just by rotating the sample. If we arrange two TURs orthogonally [21], the two modes may follow the predication of polarization independence. Fig. 7(a) and (b) shows the simulated and experimental transmission spectra of UFUR under different polarization angles θ, respectively. As the incident polarization angle θ varies from 0° to 45°, we can observe negligible difference in the transmission spectra, which clearly demonstrates the polarization-independent transmission response, similar to the property described in Ref. [21]. The experimental FWHM is 90 GHz at 0.452 THz and 80 GHz at 0.623 THz. In Fig. 7, (c) and (d) are the simulated and experimental transmission spectra of CFUR, which also present the insensitive property of the polarization angle. Compared with the UFUR, the resonant dips of CFUR are observed at two different frequencies, and exhibit a broad dip at low frequency. The coupled intensity of closed distance $s=-20$ μm is stronger than far distance $s=10$ μm. A point worth emphasizing is

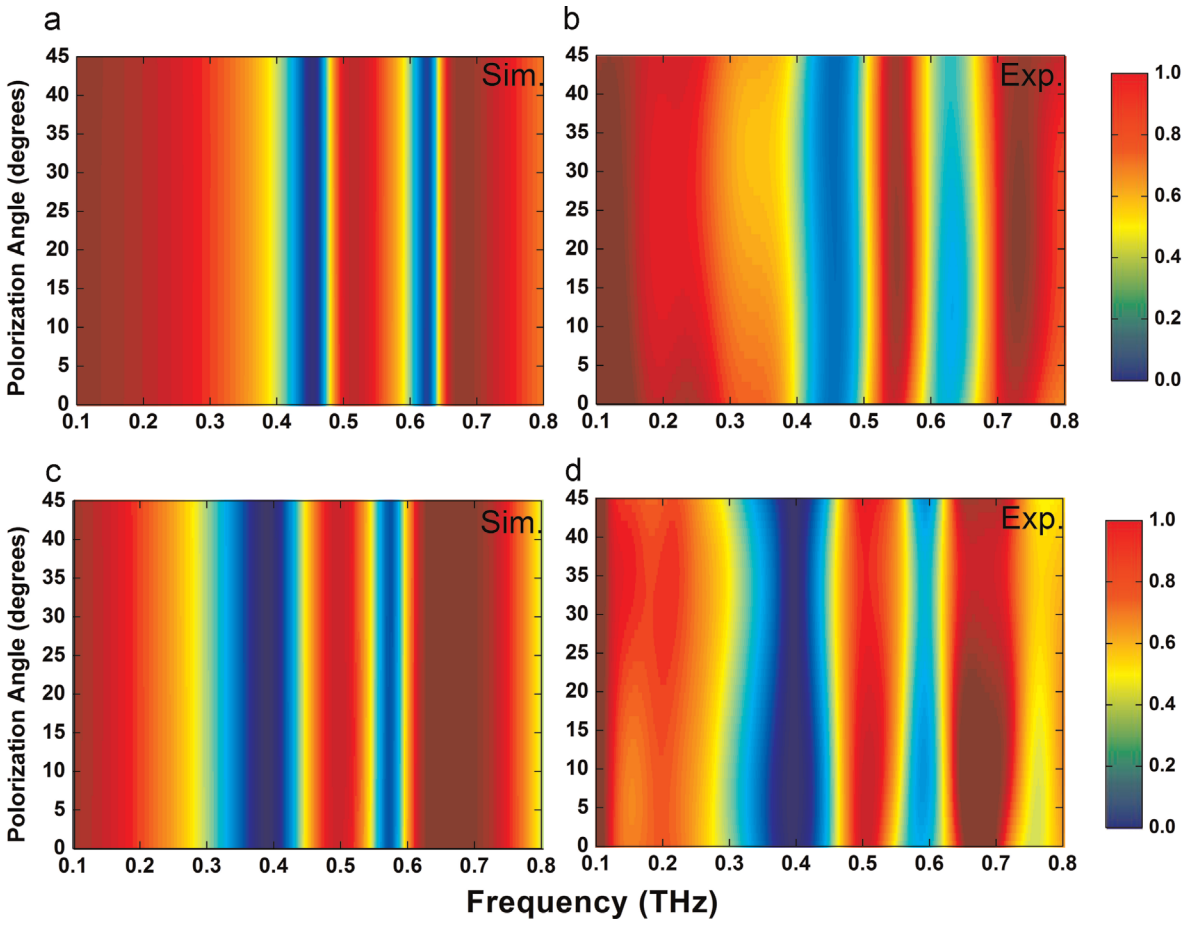

Fig. 7. (a) Simulated and (b) experimental transmission spectra of UFUR under different polarization angles θ, respectively. (c) Simulated and (d) experimental transmission spectra of CFUR under different polarization angles θ, respectively.

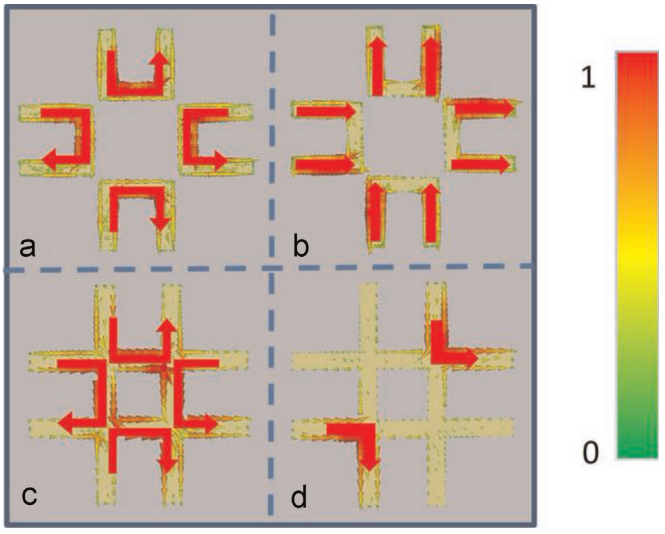

Fig. 8. Surface currents distributions of UFUR (a) 0.452 THz (low-frequency resonance dip) and (b) 0.623 THz (high-frequency resonance dip); and CFUR (c) 0.38 THz (low-frequency resonance dip) and (d) 0.56 THz (high-frequency resonance dip), when the polarization angle θ is 45°.

that the resonance modes between UFUR and CFUR are quite different, specially, an "L-shaped" resonance is observed in CFUR which does not exists in UFUR. Therefore, both the UFUR and CFUR may be applied to polarization-independent dual-channel filer.

To gain more insight of the polarization-independent property mentioned above, Fig. 8 shows the surface currents distributions of UFUR and CFUR when the polarization angle θ is 45°. At the low-frequency dip of UFUR, LC resonance can be found at the four URs concurrently, which is caused by the perpendicular electric field component to arms of each URs, shown in Fig. 8(a). The surface currents distributions of high-frequency resonance dip (see Fig. 8(b)) exhibit typical dipole resonance in all URs due to the parallel electric field component to arms. In this way, the two resonance dips always exist without a drift at any polarization angle. Thus the transmission spectra of UFUR present polarization-independent characteristics. Fig.8(c) is the surface currents distributions of CFUR at the low-frequency dip, which show LC resonance at four URs, which is similar to the condition of UFUR except a stronger resonance. However, at the high-frequency resonance dip of CFUR, two '"L-shaped" resonances emerge at neighboring arms of URs, which does not exist at UFUR. Though the polarization angle varied, the two resonant modes always generate. This is due to the fact that parallel and perpendicular electric field components invariably can be sought no matter what the polarization angle is.

5. Conclusion

In conclusion, we have proposed and demonstrated a tunable switchable modulator and a polarization-independent dual-channel filter on TUR and FUR metamaterials structures based on a flexible polyimide substrate. The modulator achieved about 0.4 peak-to-peak values at the two dips, and the FWHMs of the filter are 90 GHz and 80 GHz at the two channels for UFUR, and

130 GHz and 75 GHz for CFUR. Firstly, we discuss the fabrication of samples and present the experimental and simulated transmission responses of TUR and UFUR. Then, the electric field and surface currents distributions of these metamaterials under TM polarized wave and TE polarized wave are analyzed to show the polarization dependent property in the TUR structure. Specially, the transmission responses and resonance mechanisms of FUR with different coupled distances are discussed adequately; an "L-shaped" resonance is observed at CFUR which does not exist at UFUR. Finally, we introduce two applications based on fabricated structures, namely, a tunable switchable modulator and a polarization-independent dual-channel filter. As their special property of tunable, polarization-independent and flexible, the metamaterials structures would be widely used in THz field.

Acknowledgments

This work was partly supported by the National Program on Key Basic Research Project of China (973 Program, 2014CB339806), the Basic Research Key Project (12JC1407100), the Major National Development Project of Scientific Instrument and Equipment (2011YQ150021 and 2012YQ14000504), the National Natural Science Foundation of China (11174207, 61138001, 61205094 and 61307126), the Shanghai Rising-Star Program (14QA1403100), the Program of Shanghai Subject Chief Scientist (14XD1403000), and the New Century Excellent Talents Project from Ministry of Education (NCET-12-1052).

References

[1] P.R. Smith, D.H. Auston, M.C. Nuss, Subpicosecond photoconducting dipole antennas, IEEE J. Quantum Electron. 24 (1988) 255–260.
[2] D. Grischkowsky, S. Keiding, M.V. Exter, C. Fattinger, Far-infrared time-domain spectroscopy with terahertz beams of dielectrics and semiconductors, J. Opt. Soc. Am. B 7 (1990) 2006–2015.
[3] M. Tonouchi, Cutting-edge terahertz technology, Nat. Photon. 1 (2007) 97–105.
[4] J.S. Melinger, Y. Yang, M. Mandehgar, D. Grischkowsky, THz detection of small molecule vapors in the atmospheric transmission windows, Opt. Express 20 (2012) 6788–6807.
[5] L. Chen, Y.M. Zhu, X.F. Zang, B. Cai, Z. Li, L. Xie, S.L. Zhuang, Mode splitting transmission effect of surface wave excitation through a metal hole array, Light Sci. Appl. 2 (2013) e60.
[6] J.M. Xu, L. Chen, X.F. Zang, B. Cai, Y. Peng, Y.M. Zhu, Triple-channel terahertz filter based on mode coupling of cavities resonance system, Appl. Phys. Lett. 103 (2013) 161116.
[7] L. Chen, K.V. Truong, Z.X. Cheng, Z. Li, Y.M. Zhu, Characterization of photonic bands in metal photonic crystal slabs, Opt. Commun. 333 (2014) 232–236.
[8] S. Zhang, Y.-S. Park, J. Li, X. Lu, W. Zhang, X. Zhang, Negative refractive index in chiral metamaterials, Phys. Rev. Lett. 102 (2009) 023901.
[9] O. Paul, C. Imhof, B. Reinhard, R. Zengerle, R. Beigang, Negative index bulk metamaterial at terahertz frequencies, Opt. Express 16 (2008) 6736–6744.
[10] H. Tao, N.I. Landy, C.M. Bingham, X. Zhang, R.D. Averitt, W.J. Padilla, A metamaterial absorber for the terahertz regime: design, fabrication and characterization, Opt. Express 16 (2008) 71–81.
[11] H. Tao, C. Bingham, A. Strikwerda, D. Pilon, D. Shrekenhamer, N. Landy, K. Fan, X. Zhang, W. Padilla, R. Averitt, Highly flexible wide angle of incidence terahertz metamaterial absorber: design, fabrication, and characterization, Phys. Rev. B 78 (2008) 2–5.
[12] O. Paul, B. Reinhard, B. Krolla, R. Beigang, M. Rahm, Gradient index metamaterial based on slot elements, Appl. Phys. Lett. 96 (2010) 241110.
[13] W. Withayachumnankul, H. Lin, K. Serita, C. Shah, S. Sriram, M. Bhaskaran, M. Tonouchi, C. Fumeaux, D. Abbott, Sub-diffraction thin-film sensing with planar terahertz metamaterials, Opt. Express 20 (2012) 3345–3352.
[14] I.A.I. Al-Naib, C. Jansen, M. Koch, Thin-film sensing with planar asymmetric metamaterials resonators, Appl. Phys. Lett. 93 (2008) 083507.
[15] Z. Li, Y. Ma, R. Huang, R. Singh, J. Gu, Z. Tian, J. Han, W. Zhang, Manipulating the plasmon-induced transparency in terahertz metamaterials, Opt. Express 19 (2011) 8912–8919.
[16] Y. Ma, Z. Li, R. Huang, R. Singh, S. Zhang, J. Gu, Z. Tian, J. Han, W. Zhang, Plasmon-induced transparency in twisted Fano terahertz metamaterials, Opt. Mater. Express 1 (2011) 391–399.
[17] Z. Zhu, X. Yang, J. Gu, J. Jiang, W. Yue, Z. Tian, M. Tonouchi, J. Han, W. Zhang, Broadband plasmon induced transparency in terahertz metamaterials, Nanotechnology 24 (2013) 214003.
[18] C. Enkrich, M. Wegener, S. Linden, S. Burger, L. Zschiedrich, F. Schmidt, J. F. Zhou, T. Koschny, C.M. Soukoulis, Magnetic metamaterials at telecommunication and visible frequencies, Phys. Rev. Lett. 95 (2005) 203901.
[19] K. Aydin, I.M. Pryce, H.A. Atwater, Symmetry breaking and strong coupling in planar optical metamaterials, Opt. Express 18 (2010) 13407–13417.
[20] K.J. Chen, Z. Li, J.J. Liu, R.X. Duan, Y.Q. Wang, W. Zhang, B. Cai, L. Chen, Y.M. Zhu, A study of fss in terahertz range for polarization modulation purpose, IEEE Photon. Tech. Lett. 25 (2013) 1613.
[21] F. Zhang, Q. Zhao, J. Zhou, S. Wang, Polarization and incidence insensitive dielectric electromagnetically induced transparency metamaterial, Opt. Express 21 (2013) 19675–19680.
[22] Carsten Rockstuhl, Falk Lederer, , On the reinterpretation of resonances in split-ring-resonators at normal incidence, Opt. Express 14 (2006) 8827–8836.
[23] L. Chen, C.M. Gao, J.M. Xu, X.F. Zang, B. Cai, Y.M. Zhu, Observation of electromagnetically induced transparency-like transmission in terahertz asymmetric waveguide-cavities systems, Opt. Lett. 38 (2013) 1379–1381.
[24] L. Chen, J.M. Xu, C.M. Gao, X.F. Zang, B. Cai, Y.M. Zhu, Manipulating terahertz electromagnetic induced transparency through parallel plate waveguide cavities, Appl. Phys. Lett. 103 (2013) 251105.
[25] L. Chen, Z.X. Cheng, J.M. Xu, X.F. Zang, B. Cai, Y.M. Zhu, Controllable multiband terahertz notch filter based on a parallel plate waveguide with a single deep groove, Opt. Lett. 39 (2014) 4541–4544.
[26] L. Chen, Z.Q. Cao, F. Ou, H.G. Li, Q.S. Shen, H.C. Qiao, Observation of large positive and negative lateral shifts of a reflected beam from symmetrical metal-cladding waveguides, Opt. Lett. 32 (2007) 1432–1434.